The influence of mechanically weak layers in controlling fault kinematics and graben configurations: Examples from analog experiments and the Norwegian continental margin

Roy H. Gabrielsen, Heleen Zalmstra, Dimitrios Sokoutis, Ernst Willingshofer, Jan Inge Faleide, and Hanna Lima Braut

ABSTRACT

Fault systems in extensional basins commonly display geometries that vary with depth, reflecting depth- and lithology-dependent mechanical strength. Using an experimental approach, we investigate this relationship by deploying physical analog models with stratified sequences consisting of brittle–ductile (sand–silicone polymer) sequences subject to single and polyphase deformation. The experiments were used as analogs for a sandstone sequence interlayered by beds of evaporates or overpressured or unconsolidated mudstone in nature (the latter being representative of decollement horizons).

Experiments (series 1 [S1]) using homogeneous and stratified quartz and feldspar sand produced asymmetric, composite single grabens with diverse fault frequencies and fault styles for the graben margin faults.

For the mechanically stratified experiments with one decollement level (series 2), contrasting graben configurations were produced, in that the lowermost sequence was characterized by graben geometries of similar type to that of the S1 experiments, whereas the sequence above the decollement was characterized by large fault blocks, delineated by steepened or oversteepened faults.

The experiments with two decollements (series 3) were displayed similarly but included graben geometries that widened

Manuscript received February 6, 2017; provisional acceptance January 9, 2018; revised manuscript received March 1, 2018; revised manuscript provisional acceptance June 5, 2018; 2nd revised manuscript received July 4, 2018; final acceptance October 26, 2018.
DOI:10.1306/10261817077

AUTHORS

Roy H. Gabrielsen ~ *Department of Geosciences, University of Oslo, Oslo, Norway; r.h.gabrielsen@geo.uio.no*

Roy Helge Gabrielsen is the corresponding author of this paper. He is professor emeritus in structural geology/petroleum geology at the Department of Geosciences, University of Oslo, Norway, and was a full professor at the University of Bergen and the University of Oslo from 1989 to 2018. He has 15 years of experience as a structural geologist in the oil industry. His research interests include fault architecture and dynamics, basin formation, and the development of orogens.

Heleen Zalmstra ~ *Department of Geosciences, University of Oslo, Oslo, Norway; heleen.zalmstra@gmail.com*

Heleen Zalmstra is a structural geologist educated at Utrecht University and the University of Oslo. She is presently employed as a senior engineer at the Norwegian Mapping Authority. Her main research has been in the fields of experimental structural geology and geographical information systems.

Dimitrios Sokoutis ~ *Department of Geosciences, University of Oslo, Oslo, Norway; Faculty of Geosciences, Department of Earth Sciences, Utrecht University, Utrecht, the Netherlands; d.sokoutis@uu.nl*

Dimitrios Sokoutis is a senior researcher at the University of Utrecht, director of the tectonic laboratory, and adjunct professor at the University of Oslo. He received his Ph.D. in tectonics and geodynamics (1988) at Uppsala University, Sweden. He completed his postdoctoral studies at the University of Rennes 1, addressing the problem of postorogenic collapse. He has taught different bachelor, master, and Ph.D. courses at the University of Uppsala, Sweden; University of Rennes 1, France; University of Florence, Italy; Aristotle University of Thessaloniki, Greece; and Vrije Universiteit Amsterdam, the Netherlands.

Ernst Willingshofer ~ *Faculty of Geosciences, Department of Earth Sciences, Utrecht University, Utrecht, the Netherlands; e.willingshofer@uu.nl*

Ernst Willingshofer is a structural geologist and associate professor at Utrecht University. He fosters a multiscale approach that integrates field studies with physical analogue modeling to advance the quantitative understanding of deformation of the crust and lithosphere. Key topics include feedback relations between rheology and deformation and the importance of structural and rheological inheritance for (re)activation of deformation structures.

Jan Inge Faleide ~ *Department of Geosciences, University of Oslo, Oslo, Norway; j.i.faleide@geo.uio.no*

Jan Inge Faleide is a professor in the department of geosciences, University of Oslo. His research focuses mainly on the formation and evolution of sedimentary basins and continental margins. Most studies are located offshore of Norway and carried out in close collaboration with the petroleum industry. In these studies, geophysical and geological data are integrated at various scales, and many studies involve modeling.

Hanna Lima Braut ~ *Department of Geosciences, University of Oslo, Oslo, Norway; Aker BP, Stavanger, Norway; hannalbr@gmail.com*

Hanna Lima Braut is a structural geologist with an M.Sc. from the University of Oslo. She presently runs her own consulting company and works partly as an environmental geologist.

ACKNOWLEDGMENTS

Background for the experiments was based on seismic interpretations by Agus Fitriyanto and Aatisha Mahajan. An early version of the manuscript benefited much from careful review, thoughtful comments, and discussions with C.A.L. Jackson at Imperial College, London, and helpful reviews by Oriol Ferrer, an anonymous reviewer, and the AAPG Editor Barry J. Katz. The study is a part of the ARCEx project and was supported by the Norwegian Research Council (228107/E30) and industry partners.

upward, with each level being characterized by independent fault systems.

The results can be used to explain strata-bound fault patterns and depth-dependent extension as seen in several places along the Norwegian continental margin and elsewhere.

INTRODUCTION

Contrasting fault patterns (fault style and frequency) at different stratigraphic levels in sediment sequences caused by lithological (mechanical) strength are common in contractional (e.g., Froitzheim and Eberli, 1990; Grelaud et al., 2003; Briggs et al., 2006; Bruton et al., 2010; Chapman and McCarty, 2013; Perrin et al., 2013) as well as in extensional systems (e.g., Gabrielsen, 1984; Harvey and Stewart, 1998; Withjack and Callaway, 2000; Dooley et al., 2003; Dutton and Trudgill, 2009; Jackson and Lewis, 2012; Wilson et al., 2013; Gabrielsen et al., 2016; Ferrill et al., 2017). Decollement layers are commonly associated with distinct lithologies such as evaporite or mudstone (Brun and Choukroune, 1983; Koyi and Petersen, 1993; Stewart, 1993; Withjack and Callaway, 2000; Brun and Sokoutis, 2007; Marsh et al., 2010; Jackson and Lewis, 2012; Wilson et al., 2013). Additionally, it is locally observed that decollements are associated with distinct bedding-parallel, subhorizontal sole faults (Gabrielsen, 1984; Gibbs, 1984; Fossen and Gabrielsen, 1995; Wijns et al., 2005; Latta and Anastasio, 2007; Brun et al., 2018 and references therein). Intraformational flow in stratigraphically thick sequences, however, can create conditions in which strain is more evenly distributed within the weak unit (Edwards, 1976; Harvey and Stewart, 1998; Marsh et al., 2010; Jackson and Lewis, 2012; Anell et al., 2013; Gabrielsen et al., 2016).

Decollements in extensional fault systems are common in many basins worldwide, like in the Northern Alboran Basin in the Betics (García-Dueñas et al., 1992), the Thassos Island in Greece (Brun and Sokoutis, 2007), and the Early Cretaceous transtensional basins now exposed within the Pyrenean mountain belt (e.g., Berástegui et al., 1990). The experiments presented here were designed against the background of the Barents Sea of the Norwegian shelf, in which potential decollements are related to overpressured and unconsolidated mudstones or evaporates.

The experiments with two phases of extension are of particular interest to, for example, the Hoop fault complex of the Barents Sea (Mahajan et al., 2014; Gabrielsen et al., 2016).

Several fault systems with depth-dependent geometries are found along the Norwegian continental shelf such as the Hoop, the Ringvassøy-Loppa, and the Bjørnøya fault complexes in the Barents Sea (e.g., Gabrielsen, 1984; Gabrielsen et al., 1990, 1997, 2016; Faleide et al., 1993), the Leirfallet and Bremstein fault

complexes of mid-Norway (Marsh et al., 2010; Wilson et al., 2013), and the Egersund area of the North Sea (e.g., Kane et al., 2010; Marsh et al., 2010; Jackson and Lewis, 2013; Jackson et al., 2013; Tvedt et al., 2016). The effects of mechanically stratified sequences on fault populations at different stratigraphic levels are, therefore, well established in nature and illustrate the need for a better understanding of relationships between graben configurations and fault geometries and their vertical linkage in sedimentary sequences of mechanical contrasts.

We apply physical analog experiments to study the effects of single and polyphase extensional deformation of mechanically stratified systems with single and multiple decollement layers. These novel experiments with multiple weak beds are complementary to previously published studies using single decollements in extensional systems (e.g., Brun and Choukroune, 1983; Withjack and Callaway, 2000; Bahroudi et al., 2003; Gabrielsen et al., 2016).

SETUP AND CONDITIONS FOR THE ANALOG EXPERIMENTS

The present experiments were performed at the Tectonic Laboratory at Utrecht University and consisted of stratified brittle–ductile systems with layered sequences of sieved sand (brittle layers) of similar composition and grain size, interlayered with silicone putty (SGM-36 Dow Corning; see Weijermars et al., 1993) representing ductile layers.

All experiments were built on a 1-mm thick plastic sheet (40 × 40 cm [16 × 16 in.]) that was placed on a flat, horizontal table surface (Figure 1A). The colored layers of sieved quartz sand had a grain size of 100–300 μm, density of 1510 kgm^{-3} (3329 lbm^{-3}), cohesion of 30–70 Pa, and a coefficient of friction of 0.6. The feldspar sand had a grain size of 300 μm, cohesion of approximately 15 Pa (~0.0015 bar), and a density of 1300 kgm^{-3} (2920 lbm^{-3}). The feldspar sand grains were more angular with an internal friction coefficient of 0.75 as an average (see also Sokoutis et al., 2005; Willingshofer et al., 2005). Each silicone polymer layer was squeezed in a rolling-pin machine to obtain an equal thickness of 0.8 cm (0.3 in.) and transferred to the experiments, prior to or after the first phase of deformation.

The layered models were scaled so that 1 cm (0.4 in.) in the model approximates 1 km (0.6 mi) in nature (for scaling calculations, see McClay, 1990; Brun et al., 1994). In all cases, extension was applied by pulling a basal plastic sheet at a constant rate of 1 cm (0.4 in.)/hr. The contact between the fixed and movable base define a velocity discontinuity (VD) (Ballard et al., 1987; Tron and Brun, 1991). To avoid unwanted border effects caused by enhanced friction, care was taken to prevent silicone layers coming into direct contact with the sidewalls. The development of the experiments was documented by taking one top-view photograph for each centimeter of extension. In the experiments with two phases of extension, the first was followed by filling the surface relief with sand and smoothening it before the emplacement of a silicon polymer layer. This sequence accordingly represented a second cycle of sedimentation. Similar to the procedure described in Gabrielsen et al. (2016), sand was sieved into the developing area of subsidence during the experiments to prevent gravitational surface collapse of the graben margins and also to simulate syntectonic sedimentation. The syntectonic sand had contrasting colors to visualize the infill pattern. When complete, the experiments were covered with a monochrome layer of sand to stabilize the structures and the surface topography. Finally, the results of the experiments with one phase of extension were compared to results with two phases of extension. In both cases, the direction of extension was the same. Emphasis was paid to the reactivation of faults in response to the second phase of extension. After deformation, the models were soaked in water and cut with a knife into longitudinal stripes with a spacing of 2–5 cm (0.8–2 in.) to expose cross sections for photographs of the internal structures.

In the present analysis, the series 1 [S1] experiments, consisting of homogeneous quartz or quartz–feldspar sand sequences without a silicone polymer layer (Figure 1B), serve as a reference for experiments with one (series 2 [S2]) or two (series 3 [S3]) detachment layers of silicone (Figure 1C, D). These are relevant to the Halten terrace and the North Sea, which are both characterized by one dominant salt layer of Triassic and Permian salt, respectively (Marsh et al., 2010; Kane et al., 2010; Jackson et al., 2013; Wilson et al., 2013). The S3 experiments are of particular relevance to the Barents Sea area, because this series used two layers of mechanical contrast, which compares to the evaporite and mudstone sequences in that area (Gabrielsen et al., 2016).

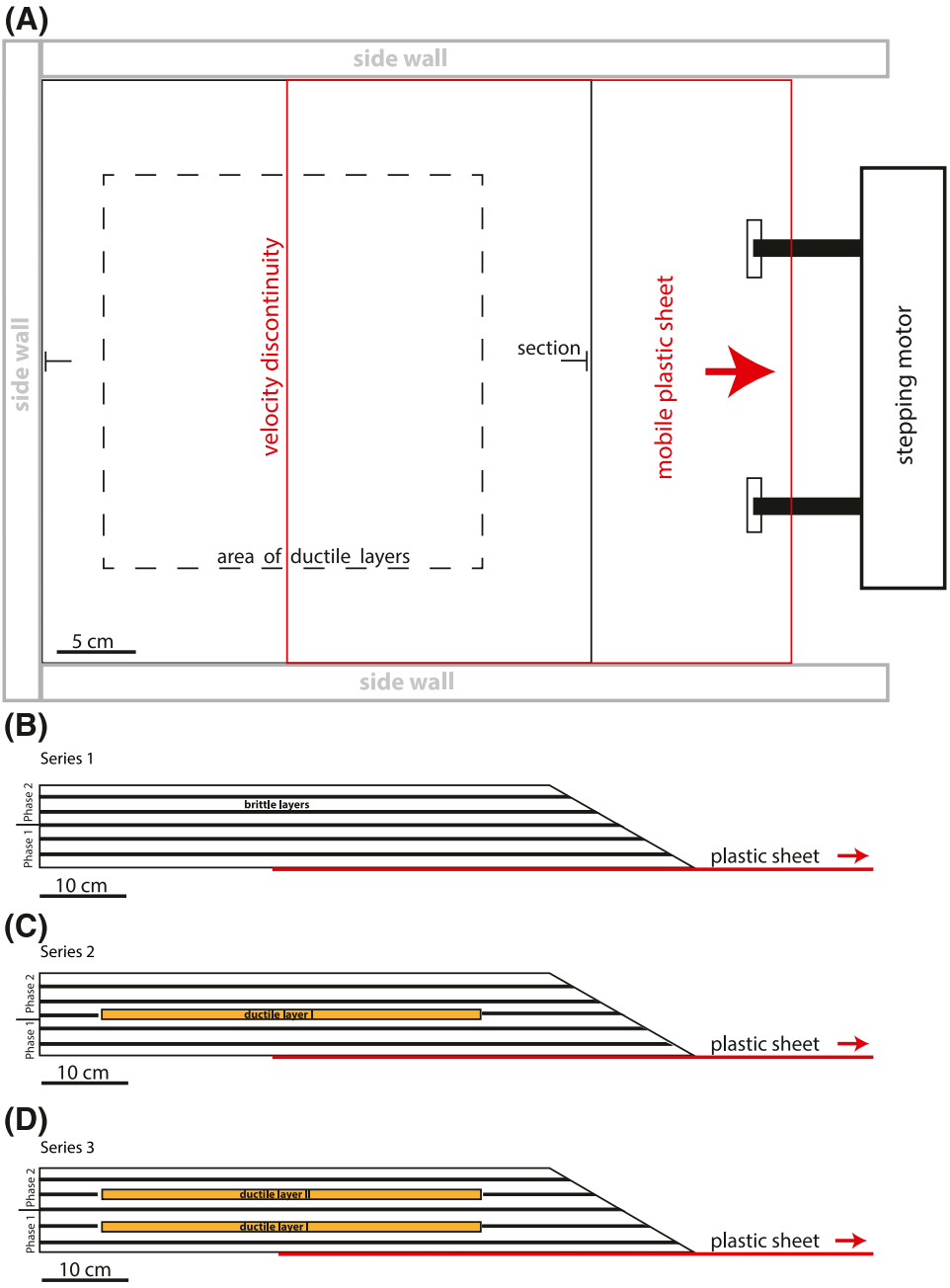

Figure 1. (A) Top view of the experimental setup. The red rectangle denotes the size and position of the plastic sheet that is pulled by the stepping motor in the direction as indicated by the red arrow. (B–D) Schematic sections showing the initial geometric and kinematic setup for experiment series 1 (only basal silicon polymer layer), series 2 (one level of silicon polymer), and series 3 (two decollement levels). In the case of polyphase extension, the morphology arising from the first phase of extension has been filled up with sediments whereupon new layers of sand and silicone related to the second phase of extension have been placed. This procedure has been applied as described and illustrated in Gabrielsen et al. (2016).

EXPERIMENTAL RESULTS

In the following sections, we describe the general development and the final geometries of each experimental series using information from individual experiments to illustrate variations among them. The part of the experiment that was positioned above the plastic base was fixed to a table so that it remained stationary throughout the experiment, whereas the other part (attached to the moving wall) was gliding

above the substratum. We refer to these blocks as "stationary" (proximal) and "moveable" (distal) blocks or segments in the descriptions below. Detailed information about the setup and conditions for each model are given in Table 1.

Experiment Series 1

Experiments in S1, which use mechanically homogeneous sand sequences, produced an overall similar structural style. As a typical example, experiment S1-1 was performed by extending by 9 cm (3.5 in.) a 10-cm (3.9-in.)-thick sequence of homogenous quartz sand in one stage, resulting in a symmetrical graben, the axis of which was oriented orthogonally to the extension direction. The first faults became visible on the surface on both sides of the subsiding graben after 1 cm (0.4 in.) of extension (Figure 2A). Normal faults continued to develop in the footwall block by sequential footwall collapse (Figure 2B–D) so that the oldest faults were found in the inner part of the graben. On the side of the moving (distal) block, deformation was focused in one relatively stable fault core that widened and accumulated the displacement, producing a more asymmetrical graben (Figure 2D). The fault array in the fixed (proximal) block were generally planar but with a listric shape toward its base.

Experiment S1-2 (Table 1) differed from S1-1 in that it used quartz sand in the lower half of the experiment and feldspar sand in the upper half, creating a strength contrast (mechanical properties of sand types are given above). Furthermore, extension was performed in two stages, during which sand was sieved into the subsiding area to prevent gravitationally induced instability (Figure 3B). Thus, after 6 cm (2.4 in.) of extension, the experiment was stopped, and a sequence of feldspar sand was sieved on top of the experiment before the second stage of extension. By the end of the second stage (6 cm [2.4 in.] of extension), the total graben width (as observed at the surface) was less than that in experiment S1-1. The cross sections displayed two fault systems that were separate in the vertical dimension. The deepest of these relates to the basin that developed in the first extension stage. This fault system was wider than the system associated with the second stage of extension affecting the shallower feldspar sand layers. Despite the mechanical discontinuity between the quartz and the feldspar units, the faults closer to the graben center that developed during the first stage of extension were reactivated during the second stage, propagating upwards. In contrast, the marginal (distal) faults in the stationary wall of the experiments remained isolated and inert during the second stage.

Experiment Series 2

After the first stage of extension, the experiment of S2 was halted, its surface was smoothed with sand, and a silicon layer of equal thickness (0.8 cm [0.3 in.]) was deposited. In the first stage of these experiments, an

Table 1. Summary of Setup and Conditions for Experiments Used in the Present Analysis

Expr. Series	Expr. No.	Materials	Sequence Thickness, cm (in.)	Silicone Polym. Layer Thickness, cm (in.)	Depth of SP Layer, cm (in.)	Phases of Extension	Total Extension, cm (in.)
1	1	Qtz sand	9.6 (3.8)	None	–	1	9 (3.5)
	4	Qtz sand fsp sand	10.0 (3.9)	None	–	2	6 + 6 (2.3 + 2.3)
2	2	Qtz sand one sp layer	10.4 (4.1)	0.8 (0.3)	4.8 (1.89)	1	5 (2.0)
	3	Qtz sand one sp layer	10.4 (4.1)	0.8 (0.3)	4.8 (1.89)	2	4 + 3 (1.6 + 1.2)
	8	Qtz sand one sp layer glass beads	10.0 (3.9)	0.4 (0.16)	6.6 (2.6)	2	2 + 2 (0.8 + 0.8)
3	5	Qtz sand two sp layers	9.8 (3.85)	0.4 (0.16)	3.0 and 0.6 (1.18 and 0.28)	1	4 (1.6)
	6	Qtz sand two sp layers	9.8 (3.85)	0.4 (0.16)	3.0 and 0.6 (1.18 and 0.28)	2	2 + 2 (0.8 + 0.8)
	7	Qtz sand two sp layers	9.8 (3.85)	0.4 (0.16)	3.0 and 0.6 (1.18 and 0.28)	2	2 + 2 (0.8 + 0.8)

The experiments were divided into three series: series 1 consisted of sand only; series 2 and 3 used one and two layers of silicon polymer, respectively. The experiments were performed with single and polyphase extension and different bulk extension (columns 7 and 8).

Abbreviations: – = not available; Expr. = experiment; fsp = feldspar; No. = number; Polym. = polymer; qtz = quartz; sp = silicon polymer.

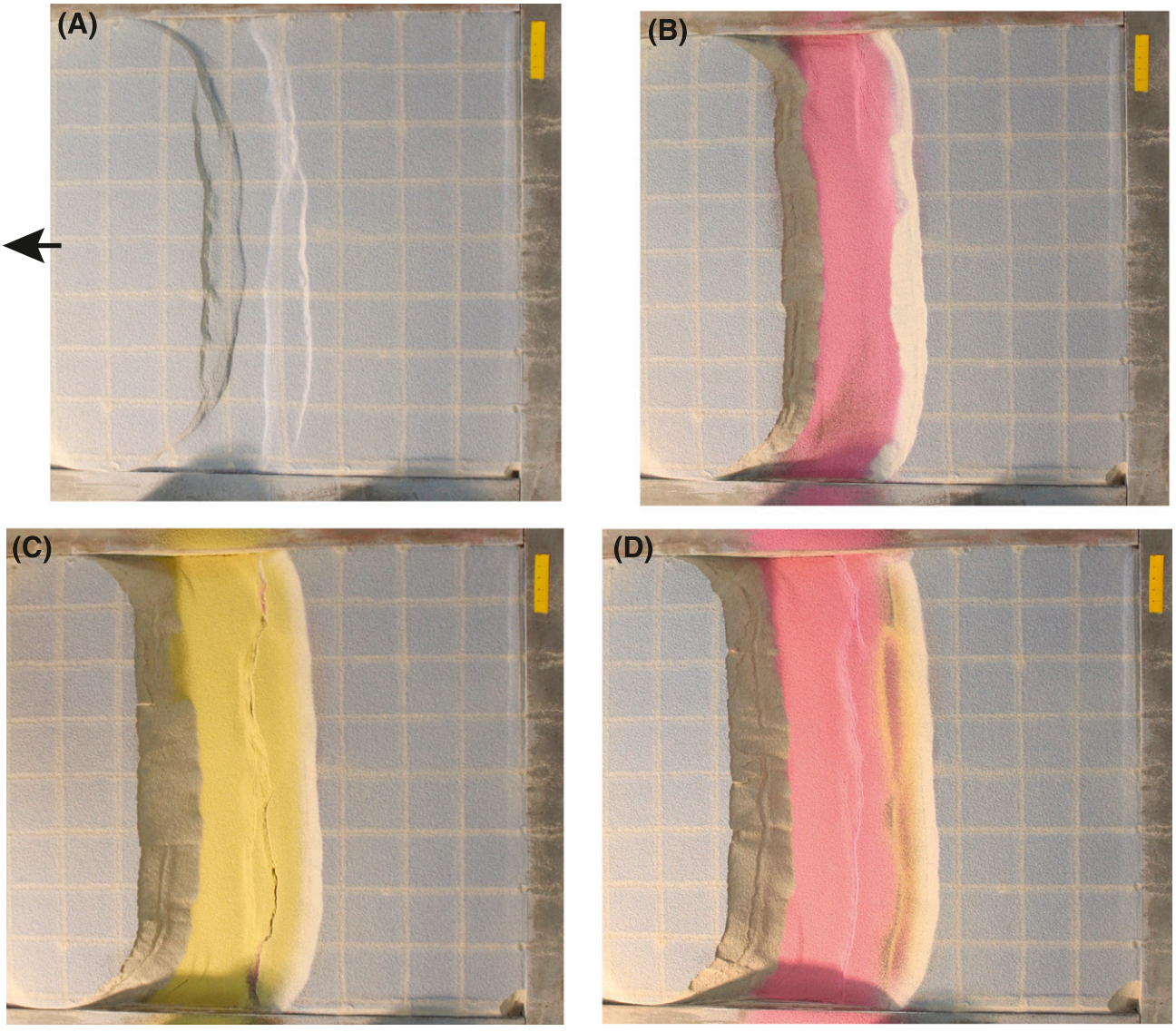

Figure 2. (A–D) Top-view photographs showing the stepwise development of experiment S1-1 after extensions of (A) 1 cm (0.4 in.), (B) 3 cm (1.2 in.), (C) 5 cm (1.9 in.), and (D) 7 cm (2.8 in.). The arrow indicates the direction of the moving block. Grid spacing is 4 cm (1.6 in.).

asymmetrical graben with an array of antithetic faults facing the graben axis developed in the fixed (proximal) fault block and one stable synthetic fault with one fault core 0.5 cm (0.2 in.) in width facing the graben axis developed in the moving (distal) block were produced (Figure 4). The three experiments of S2 displayed almost identical development and final geometries (Figure 4).

After depositing the silicone polymer layer and the upper sand sequence, extension was restarted. In all S2 experiments, an elongated sag area started to develop orthogonally and above the buried graben axis (VD) from the first deformation stage. As seen on the surface, the second stage of the S2 experiment was characterized by a much wider, asymmetric horst-and-graben system with a central half graben situated above a wide, broken (Figure 4A), or intact (Figure 4B) fault block that rotated toward the graben axis. The large fault blocks were delineated by rotating normal faults. These confined fault blocks were sliding on top of the upper silicone polymer layer toward the graben center (Figure 4). All faults in this stage were rooted in the silicon polymer layer and were generally not coupled with the faults of stage 1. The only exception from this was the border faults that were semicoupled to the deeper faults. This type of configuration was observed in all S2 experiments. All faults in the upper fault system were planar,

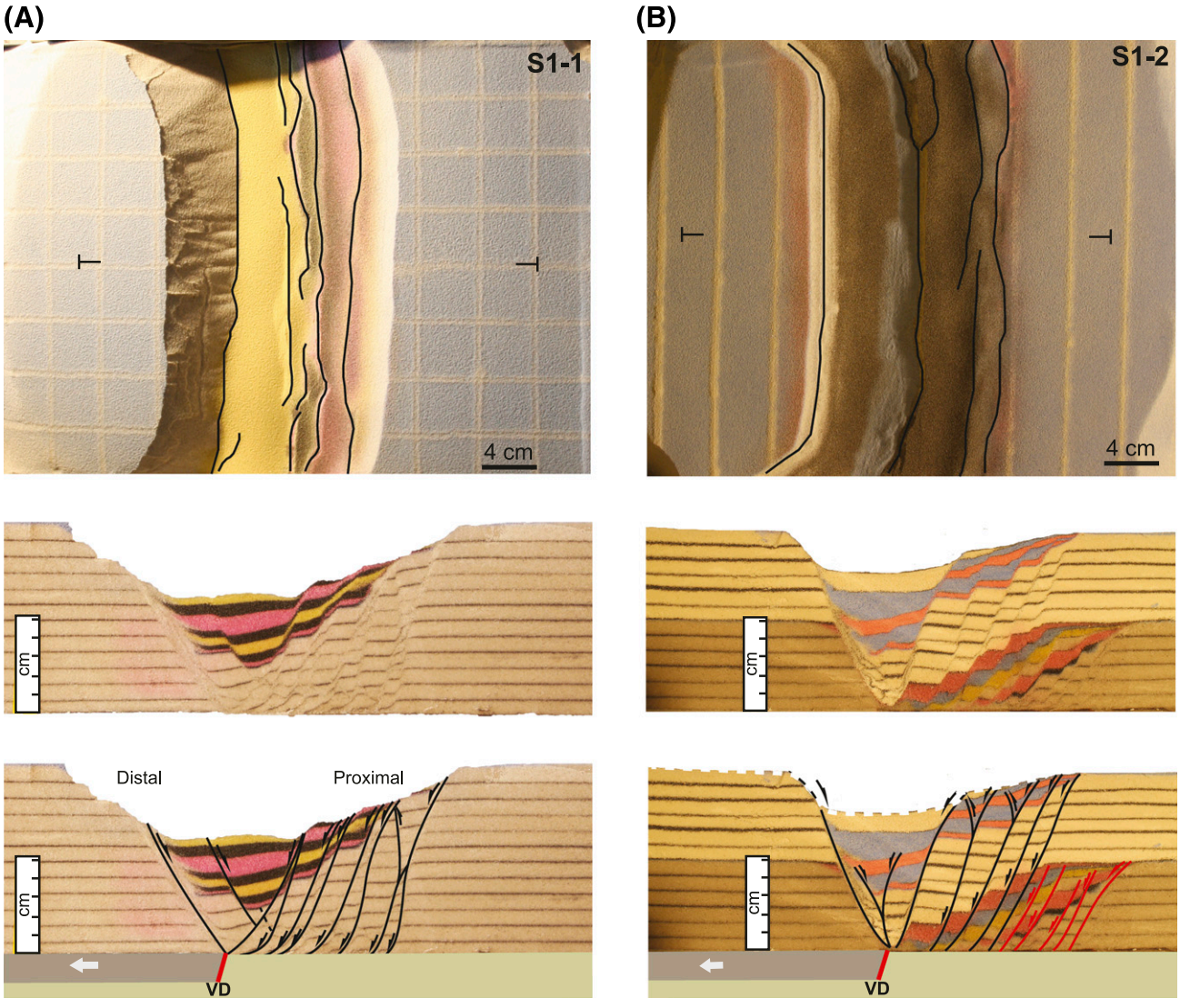

Figure 3. Top views and cross sections of experiments in series 1 (S1), S1-1 and S1-2, portraying the finite geometry of the models (after 9 cm [3.5 in.] of extension). (A) Experiment S1-1 was performed with only quartz sand and one stage of extension. Note different fault styles for the two-graben margins. (B) Experiment S1-2 was performed with quartz sand in the first stage (base; gray) and feldspar sand (top; white) in the second stage. Note the wider area of faulting associated with the first stage compared to the narrower graben associated with the second stage of extension. See text for full description. The gray surface represents the movable sheet, which has been pulled in the direction of the arrow. VD = velocity discontinuity.

except for those in the middle graben that were upward steepening.

Experiment Series 3

In this series of experiments, a second ductile layer with similar mechanical properties and dimensions to that used in S2 was included so that the two layers were situated 30 and 66 mm (1.2 and 2.6 in.) above the base of the model (Figure 1; Table 1). In experiment S3-1, the model was extended in one stage, whereas two phases of 2-cm (0.8-in.) extension were used in experiments S3-2 and S3-3, with the upper layer placed after the first phase of extension.

All experiments produced a shallow syncline after 6% extension, which became bordered by two separate, narrow grabens. The first faults appeared at the surface on the side of the stable block of the sag area after 10% of extension, whereas the earliest faults on the opposite side of the sag area appeared slightly later. The graben units became segmented by continued extension and subsided in concert until the termination of the experiment.

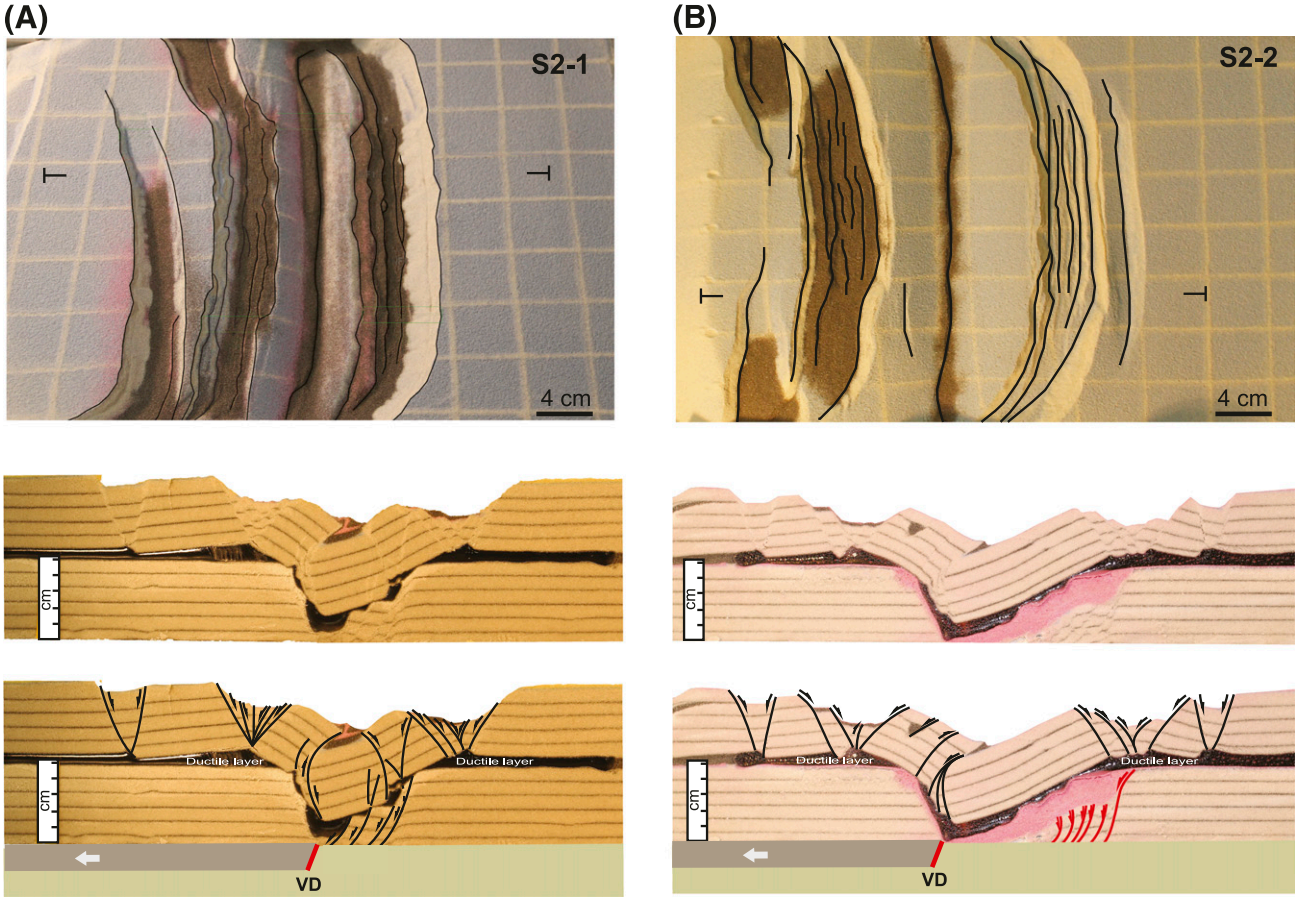

Figure 4. Oblique and top view and cross sections showing the finite geometries of series 2 (S2) experiments: (A) S2-1 and (B) S2-2. These experiments were performed with one layer of silicon putty separating a lower and an upper sand sequence. Both sequences were quartz sand. Note contrast in graben geometry between stages 1 and 2, the complex system of lined grabens, and the large, basinward-rotated fault block that was common for stage 2 for all experiments. VD = velocity discontinuity.

The profiles show that the structures were asymmetrical grabens, characterized by a contrasting number of faults at the two flanks. Thus, the stationary block developed one master fault that absorbed the entire extension on the distal side. The moving block, however, was characterized by the sequential development of an array of parallel, normal faults. In some experiments, the graben flanks developed rafts sliding on the uppermost ductile layer causing local reverse faulting (Figure 4). The central part of these grabens was situated right above the basal VD. This is identical to what was observed in the S1 and the first stage of the S2 experiments.

The second stage of extension produced similar, but wider structures in the two upper sand layers, as compared to the ones of the deepest sand layer. The faults displayed both coupled and semicoupled (Jackson and Lewis, 2013) relationships between levels 1 and 2 and between levels 2 and 3, respectively (Figure 5). The hard-linked faults mainly occurred in the boundary faults of the graben.

The experiments of S3 were stopped by a total extension of 4 cm (1.6 in.) because the lowermost sequence was thinned to less than 1 cm (<0.4 in.).

In summary, it was observed that when adding a second ductile layer and the upper sequence of sand (e.g., experiment S3-2) three distinct, separate stratabound fault systems formed (Figure 5). The graben structures widened stepwise from the bottom to the top sand sequences. As in the experiments of the two previous series, the deepest fault system generated an asymmetric graben. In contrast, the middle and upper sand units were delineated by symmetric grabens. The faults were generally planar. Exceptions were upward-steepening faults, which were related to the rotation of the marginal fault blocks.

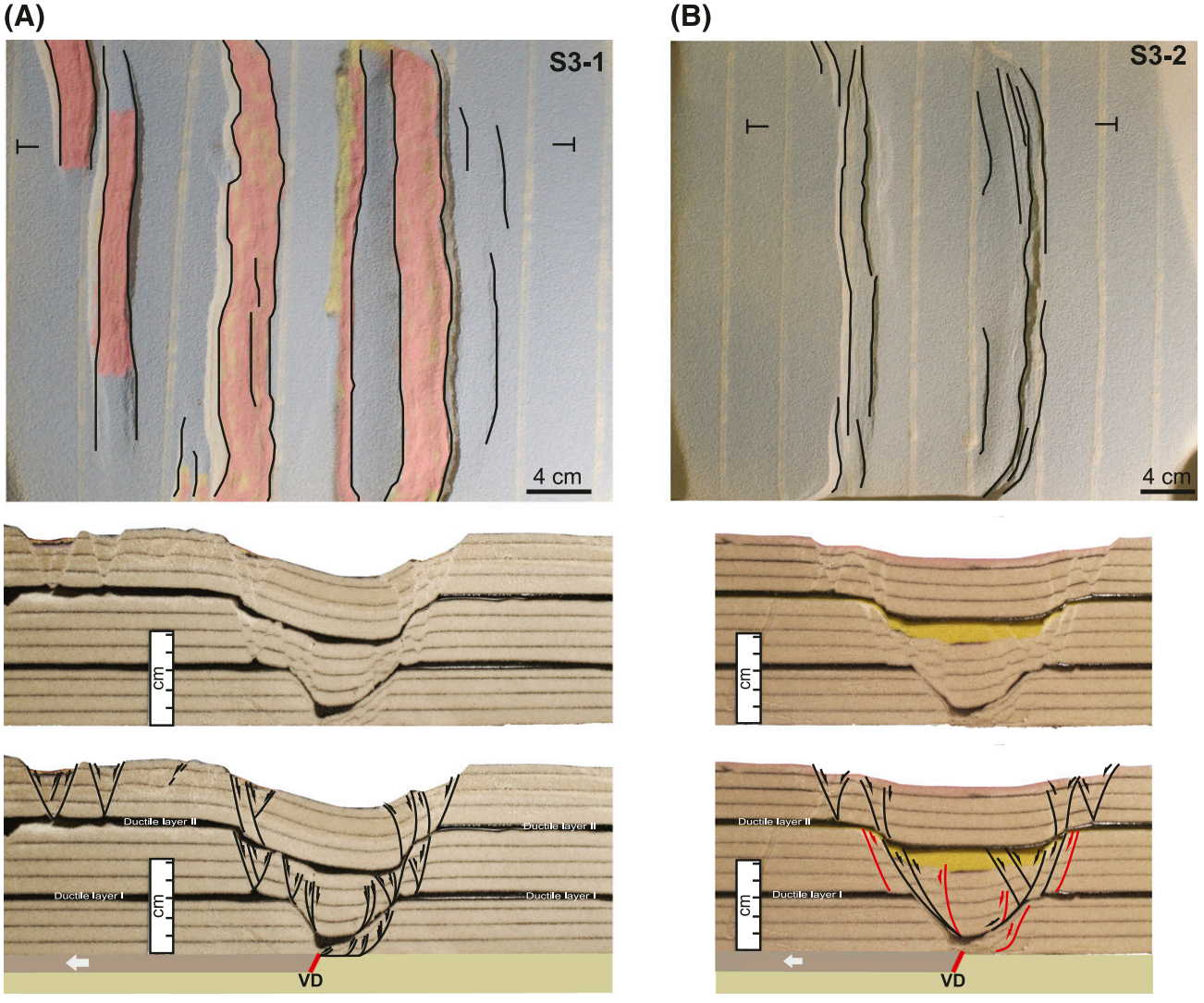

Figure 5. Map view and cross sections of series 3 (S3) experiments, S3-1 and S3-2 (two layers of silicon polymer separating three sequences of quartz sand). Note the generally symmetrical grabens at all levels and the upward increasing graben width. VD = velocity discontinuity.

DISCUSSION AND EXAMPLES

The present experiments demonstrated the influence of multiple decollement horizons on basin (graben) formation as well as on fault styles and fault-linking or coupling mechanisms in stacked sediment sequences. The present experiments have also shown that fault and graben geometries may be influenced by minor and major mechanical contrasts (e.g., quartz–feldspar sand, sand–silicone polymer) to a variable extent as also commonly seen in nature (e.g., Ferrill et al., 2017). Such complexity increases for systems with multiple decollement horizons and polyphase deformation (see also Brun and Choukroune, 1983; Harvey and Stewart, 1998; Withjack and Callaway, 2000; Gabrielsen et al., 2016). This is also similar to that reported for contractional systems in Soleimany et al. (2013) and Santolaria et al. (2015).

Thus, the experiments performed with a mechanically homogeneous sequence (i.e., experiment S1-1; quartz sand) and one stage of extension displayed a graben asymmetry in an array of subparallel extensional planar faults with the listric lowermost parts developed in the stationary fault block. The combined planar (upper) and listric (lower) geometries of these faults are most likely caused by frictional drag at the base of the fault block. In contrast, the

displaced block developed a zone with one dominant fault and a widening fault core that remained stable throughout the experiments (Figure 6A). This geometry was probably ruled by the displacement of the basal VD.

The stratified experiment S1-2 (quartz and feldspar sand) resulted in an up-section narrowing of the graben width (in the feldspar sand sequence). This may be influenced by strength contrast (greater friction) in the sand column, but it is more likely controlled by the vertical and horizontal distances to the VD itself. This means that up-section–narrowing graben systems can be expected in sedimentary sequences of inverted mechanical strength and with increasing distance from the VD and that the commonly observed downward narrowing in multistage grabens may be promoted by compaction and increasing mechanical strength with depth.

When one silicon putty layer was introduced between the sand sequences, two distinct intraformational vertically coupled or semicoupled fault systems (below and above the silicone polymer layer) formed. In these experiments, the fault system associated with the deeper sand layer was similar to that developed during S1 (sand sequences without the silicon putty layer). The fault system affiliated with the second extension stage (above the decollement layer) displayed a strikingly different development and geometry. In contrast to S1, the deformation in S2 activated a wider panel above the decollement than below it (stage 1) and included some upward-steepening faults defining reverse faults. Such geometries are promoted by strong contrasts in mechanical stiffness in which the stronger layer is the deepest (Horsfield, 1977; Withjack and Callaway, 2000). The reason for this geometry in this case, is, however, that the faults of the upper sequence were associated with basinward–sliding fault blocks that had been trapped at the margins of the first-stage graben structures where the silicon polymer layer had been substantially thinned or welded. Such structures are commonly seen in connection with salt tectonics (Figure 4). Such unstable, sliding fault blocks on basin margins are known from several places at the mid-Norwegian continental shelf (e.g., the Mikkel structure [Withjack and Callaway, 2000] and Revfallet fault complex [Dooley et al., 2003]). Hence, the fault pattern of the upper sand sequence was completely different from that of the lowermost sand unit. Although not very common, such geometries are found in several places in the vicinity of basins with active synfaulting halokinesis (Harvey and Stewart, 1998). One example from the Vingleia fault complex of mid-Norway is shown in Figure 6B.

By adding a second ductile layer, a third stratabound fault population developed in the uppermost brittle unit. The faults and the master faults at the uppermost level had either coupled or semicoupled relationships to faults at deeper levels (Figure 5), allowing for differential strain to be accumulated for each layer. However, most faults in each sand unit seemed to be nucleated at the lower contact between the silicon putty and the sand, in some cases generating blind faults. Contrasts in fault frequency and style when comparing the deep and shallow sand sequences separated by silicon putty as observed in the experiments of S2 and S3 are similar to observations reported for natural fault systems by the Channel Basin of southern England (Harvey and Stewart, 1998), the Bremstein and Revfallet fault complexes offshore mid-Norway (Dooley et al., 2003; Wilson et al., 2013), the Sembo relay system offshore Angola (Dutton and Trudgill, 2009), and for several fault systems elsewhere (Withjack and Callaway, 2000).

By further extension, it is likely that the master fault systems in these arrays would become hard linked in the vertical dimension, generating a consistent system of faults like that reported by Harvey and Stewart (1998), Jackson and Lewis (2012), Jackson et al. (2013), and Gabrielsen et al. (2016). In experiments S2 and S3, vertical fault linkage was promoted where layers of silicone polymer remained intact. Accumulated heave was associated with repeated reactivation as reported from the Barents Sea by Mahajan et al. (2014). This observation is also consistent with analog experimental results obtained by Withjack and Callaway (2000) and Dooley et al. (2003) (Figure 6C). In cases in which the silicon polymer became unevenly thinned and even thinned to zero, vertically stacked regimes of contrasting geometry and the rotation of fault blocks toward the basin center was common, with the fault block riders sometimes becoming stuck at the graben margins where the silicon polymer was thinned the most (Figure 6B).

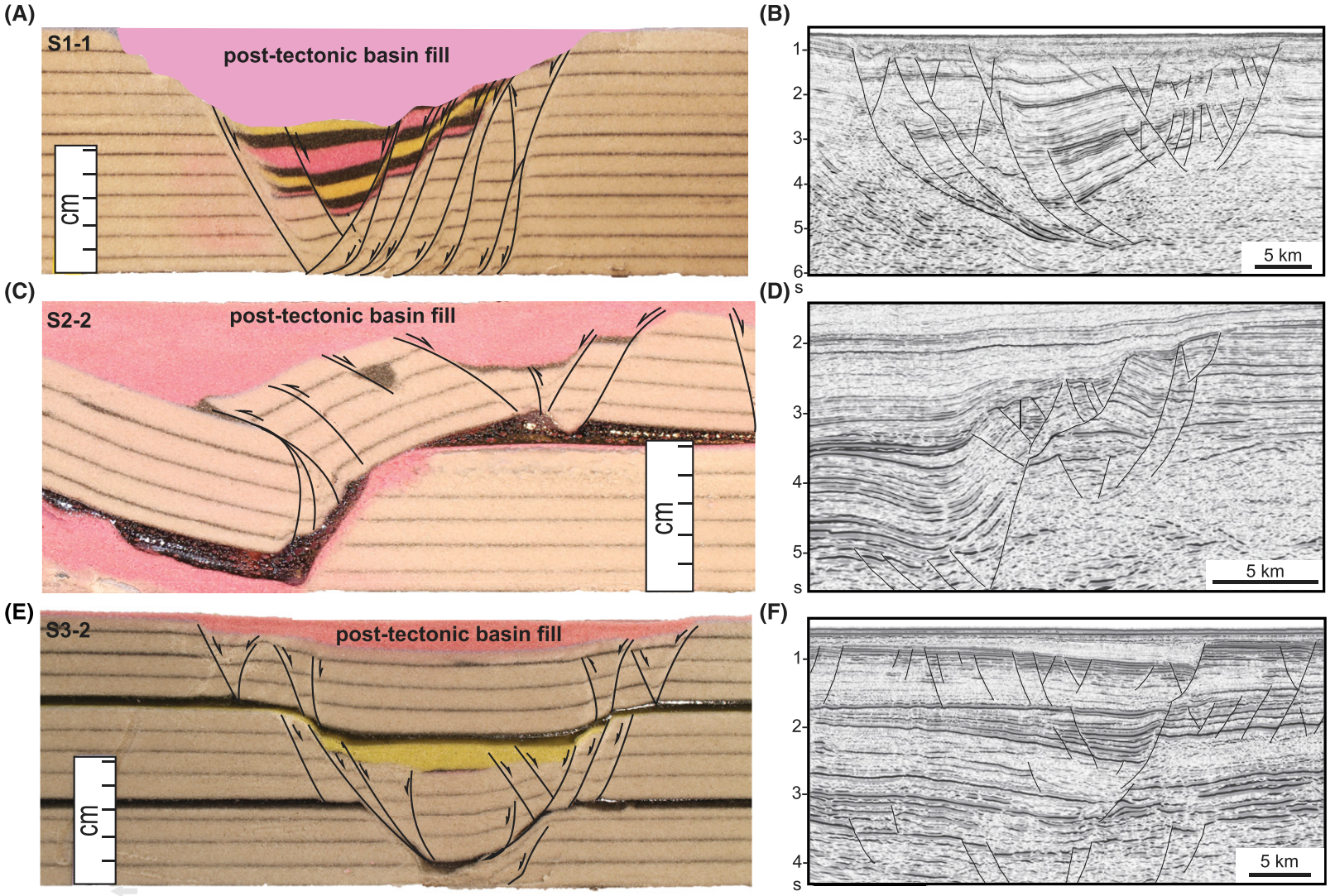

Figure 6. Comparison between experiments and observed fault and graben geometries at the Norwegian continental shelf. (A, B) Graben with contrasting fault geometry at the two margins. Series 1 (S1) experiment S1-1 and seismic example from the margin of the Fingerdjupet subbasin, southwestern Barents Sea (modified from Norkus, 2015). (C, D) Upward-steepening antilistric fault at the graben margin with a sliding fault block. Series 2 (S2) experiment S2-2 and seismic example from the Bremstein fault complex offshore, mid-Norway (modified from Avaldsnes, 2014). (E, F) Graben systems developed above weak layers where graben marginal fault steps toward the footwall for each structural level, resulting in stepwise increasing the up-section graben width. Series 3 (S3) experiment S3-6 and seismic example from the Hoop fault complex, southwestern Barents Sea (modified from Fitriyanto, 2011). Seismic data courtesy of TGS and Spectrum.

CONCLUSIONS

The three series of experiments shed light on the mechanisms leading to composite and complex fault geometries sometimes observed in reflection seismic data, demonstrating the following results.

1. The deepest fault system developed in homogeneous quartz sand produced a very robust and asymmetric graben geometry with deformation being localized along a wide and diffuse fault at the moving (distal with respect to the stationary fault block) flank of the graben, whereas strain was distributed over several discrete faults at the stationary proximal) flank. This development was similar for all one-stage experiments and for the first stage in multistage experiments.
2. In experiments with one or several decollement layers, fault systems of the middle and upper sand units (above silicon putty layers) had significantly different configurations from the fault systems in the layers below the decollement. For the three-layer (sand/silicon/sand) system, configurations were dramatically different for the two sand sequences. In these experiments, large, rotated fault blocks delineated by antilistric faults with a reverse throw developed above the graben margin master faults. These were affected by gravitationally induced sliding of the fault blocks across the deeper graben margins. The fault systems in deep and shallow sequences were generally unlinked. It is inferred that this pattern is strongly influenced by the gravitational forces because of basinward sliding of the uppermost fault block
3. The three-layer systems produced relatively symmetrical upward-widening graben structures with a stronger tendency for soft linking and hard linking between the deep and shallow faults, generating more stable but upward-widening graben structures. The gravitational component causing basinward fault block sliding was less pronounced in these experiments.
4. We find that some of the depth-dependent and composite graben geometries as well as complex fault geometries developed in the present experiments explains some less well-explained geometries in extensional structures observed in the Norwegian continental shelf.

REFERENCES CITED

Anell, I., A. Braathen, S. Olaussen, and P. T. Osmundsen, 2013, Evidence of faulting contradicts a quiscent northern Barents Shelf during the Triassic: First Break, v. 31, p. 67–76.

Avaldsnes, R. R., 2014, Structure and evolution of the Bremstein fault complex offshore mid-Norway, M.Sc. thesis, University of Oslo, Oslo, Norway, 88 p.

Bahroudi, A., H. A. Koyi, and C. J. Talbot, 2003, Effect of ductile and frictional décollements on style of extension: Journal of Structural Geology, v. 25, no. 9, p. 1401–1423.

Ballard, J-F., J.-P. Brun, J. Van den Driessche, and P. Allemand, 1987, Propagation des chevauchements au-dessus des zones de décollement: Modèles expérimentaux: Comptes Rendus de l'Académie des Sciences, v. 11, no. 305, p. 1249–1253.

Berástegui, X., J. M. García-Senz, and M. Losantos, 1990, Tectosedimentary evolution of the Organya extensional basin (central south Pyrenean unit, Spain) during the Lower Cretaceous: Bulletin de la Société Geologiue de France, v. 6, no. 2, p. 251–264, doi:10.2113/gssgfbull.VI.2.251.

Briggs, S. E., R. J. Davies, J. A. Cartwright, and R. Morgan, 2006, Multiple detachment levels and their control on fold styles in the compressional domain of the deepwater west Niger Delta: Basin Research, v. 18, no. 4, p. 435–450.

Brun, J.-P., and P. Choukroune, 1983, Normal faulting, block tilting, and décollement in a stretched crust: Tectonics, v. 2, no. 4, p. 345–356.

Brun, J.-P., and D. Sokoutis, 2007, Kinematics of the southern Rhodope Core Complex (North Greece): International Journal of Earth Sciences, v. 96, p. 1079–1099, doi: 10.1007/s00531-007-0174-2.

Brun, J.-P., D. Sokoutis, C. Tirel, F. Gueydan, J. Van den Driessche, and M.-O. Beslier, 2018, Crustal versus mantle core complexes: Tectonophysics, v. 746, p. 22–45, doi:10.1016/j.tecto.2017.09.017.

Brun, J.-P., D. Sokoutis, and J. Van den Driessche, 1994, Analogue modeling of detachment fault systems and core complexes: Geology, v. 22, p. 319–322.

Bruton, D. L., R. H. Gabrielsen, and B. T. Larsen, 2010, The Caledonides of the Oslo Region, Norway – stratigraphy and structural elements: Norwegian Journal of Geology, v. 90, p. 93–121.

Chapman, J. B., and R. S. McCarty, 2013, Detachment levels in the Marathon fold and thrust belt, west Texas: Journal of Structural Geology, v. 49, p. 23–34, doi:10.1016/j.jsg.2013.01.007.

Dooley, T., K. R. McClay, and R. Pascoe, 2003, 3D analogue models of variable displacement extensional faults: Applications to the Revfallet Fault system, offshore mid-Norway: Geological Society, London, Special Publications 2003, v. 212, p. 151–167, doi:10.1144/GSL.SP.2003.212.01.10.

Dutton, D.M., and B.D Trudgill, 2009, Four-dimensional analysis of the Sembo relay system, offshore Angola: Implications for fault growth in salt-detached settings: AAPG Bulletin, v. 93, no. 6, p.763-794, doi:10.1306/02230908094.

Edwards, M. B., 1976, Growth faults in Upper Triassic deltaic sediments, Svalbard: AAPG Bulletin, v. 60, no. 3, p. 341–355.

Faleide, J. I., E. Vågnes, and S. T. Gudlaugsson, 1993, Late Mesozoic-Cenozoic evolution of the south-western Barents Sea in a regional rift-shear tectonic setting: Marine and Petroleum Geology, v. 10, p. 186–214, doi:10.1016/0264-8172(93)90104-Z.

Ferrill, D. A., A. P. Morris, R. N. McGinnis, K. J. Smart, S. S. Wigginton, and N. J. Hill, 2017, Mechanical stratigraphy and normal faulting: Journal of Structural Geology, v. 94, p. 275–302, doi:10.1016/j.jsg.2016.11.010.

Fitriyanto, A., 2011, Structural analysis of the Hoop fault complex, SW Barent Sea, M.Sc. thesis, University of Oslo, Oslo, Norway, 83 p.

Fossen, H., and R. H. Gabrielsen, 1995, Experimental modeling of extensional fault systems by use of plaster: Journal of Structural Geology, v. 18, no. 5, p. 673–687, doi:10.1016/S0191-8141(96)80032-0.

Froitzheim, N., and G. P. Eberli, 1990, Extensional detachment faulting in the evolution of a Tethys passive continental margin, Eastern Alps, Switzerland: Geological Society of America Bulletin, v. 102, no. 9, p. 1297–1308, doi:10.1130/0016-7606(1990)102<1297:EDFITE>2.3.CO;2.

Gabrielsen, R. H., 1984, Long-lived fault zones and their influence on the development of the southwestern Barents Sea: Journal of the Geological Society, v. 141, no. 4, p. 651–662, doi:10.1144/gsjgs.141.4.0651.

Gabrielsen, R. H., R. B. Færseth, L. N. Jensen, J. E. Kalheim, and F. Riis, 1990, Structural elements of the Norwegian Continental Shelf. Part I: The Barents Sea Region: Stavenger, Norway, Norwegian Petroleum Directorate 256, Bulletin 6, p. 1–33, http://www.npd.no/Global/Norsk/3-Publikasjoner/NPD-Bulletin/NPD_BulletinNr6.pdf.

Gabrielsen, R. H., I. Grunnaleite, and E. Rasmussen, 1997, Cretaceous and tertiary inversion in the Bjørnøyrenna Fault Complex, south-western Barents Sea: Marine and Petroleum Geology, v. 14, no. 2, p. 165–178, doi:10.1016/S0264-8172(96)00064-5.

Gabrielsen, R. H., D. Sokoutis, E. Willingshofer, and J. I. Faleide, 2016, Fault linkage across weak layers during extension: An experimental approach and consequence in the Hoop Fault Complex of the southeastern Barents Sea: Petroleum Geoscience, v. 22, no. 2, p. 123–135, doi:10.1144/petgeo2015-029.

García-Dueñas, V., J. C. Balanyá, and J. M. Martínez-Martínez, 1992, Miocene extensional detachments in the outcropping basement of the Northern Alboran Basin (Betics) and their tectonic implications: Geo-Marine Letters, v. 12, no. 2–3, p. 88–95, doi:10.1007/BF02084917.

Gibbs, A. D., 1984, Structural evolution of extensional basin margins: Journal of the Geological Society, v. 141, no. 4, p. 609–620, doi:10.1144/gsjgs.141.4.0609.

Grelaud, S., J. Vergés, T. Nalpas, and R. Karpuz, 2003, Impact of multiple detachment levels on deformation of external fold-and-thrust belts (abs.): EGS-AGU-EUG Joint Assembly, Nice, France, April 6–11, 2003, 1 p.

Harvey, M. J., and S. A. Stewart, 1998, Influence of salt on the structural evolution of the Channel Basin: Geological Society, London, Special Publications 1998, v. 133, p. 241–266.

Horsfield, W. T., 1977, An experimental approach to basement-controlled faulting: Geologie en Mijnbouw, v. 56, no. 4, p. 363–370.

Jackson, C. A.-L., S.-T. Chua, R. E. Bell, and C. Magee, 2013, Structural style and early stage growth of inversion structures: 3D seismic insights from the Egersund Basin, offshore Norway: Journal of Structural Geology, v. 46, p. 167–185, doi:10.1016/j.jsg.2012.09.005.

Jackson, C. A.-L., and M. M. Lewis, 2012, Origin of an anhydrite sheath encircling a salt diapir and implications for the seismic imaging of steep-sided salt structures, Egersund Basin, Northern North Sea: Journal of the Geological Society, v. 169, no. 5, p. 593–599, doi:10.1144/0016-76482011-126.

Jackson, C. A.-L., and M. M. Lewis, 2013, Physiography of the NE margin of the Permian Salt Basin: New insights from 3D seismic reflection data: Journal of the Geological Society, v. 170, no. 6, p. 857–860, doi:10.1144/jgs2013-026.

Kane, K. E., C.A.-L. Jackson, and E. Larsen, 2010, Normal fault growth and fault-related folding in a salt-influenced rift basin: South Viking Graben, offshore Norway: Journal of Structural Geology, v. 32, p. 490–506, doi:10.1016/j.jsg.2010.02.005.

Koyi, H., and K. Petersen, 1993, Influence of basement faults on the development of salt structures in the Danish Basin: Marine and Petroleum Geology, v. 10, no. 2, p. 82–94, doi:10.1016/0264-8172(93)90015-K.

Latta, D. K., and D. J. Anastasio, 2007, Multiple scales of mechanical stratification and décollement fold kinematics, Sierra Madre Oriental foreland, northeast Mexico: Journal of Structural Geology, v. 29, no. 7, p. 1241–1255, doi:10.1016/j.jsg.2007.03.012.

Mahajan, A., R. H. Gabrielsen, and J. I. Faleide, 2014, Structural analysis of 3D seismic for the Hoop Fault Complex, SW Barents Sea (abs.), *in* S. Eriksen, H. Haflidason, O. Olesen, H. Schiellerup, and A. M. Husås, eds., The Arctic Days Conference: Abstracts and Proceedings of the Geological Society of Norway, Moscow, November 20–22, 2014, v. 2, p. 58.

Marsh, N., J. Imber, R. E. Holdsworth, P. Brockbank, and P. Ringrose, 2010, The structural evolution of the Halten Terrace, offshore Mid-Norway: Extensional fault growth and strain localisation in a multi-layer brittle–ductile system: Basin Research, v. 22, no. 2, p. 195–214, doi:10.1111/j.1365-2117.2009.00404.x.

McClay, K. R., 1990, Extensional fault systems in sedimentary basins: A review of analogue model studies: Marine and Petroleum Geology, v. 7, p. 206–233; doi:1016/0264-8172(90)90001-W.

Norkus, A., 2015, Pre-Jurassic evolution of the Fingerdjupet subbasin, SW Barents Sea, M.Sc. thesis, University of Oslo, Oslo, Norway, 82 p.

Perrin, C., L. Clemenzi, J. Malaveille, G. Molli, A. Taboda, and S. Dominguez, 2013, Impact of erosion and décollements on large-scale faulting and folding in orogenic wedges: Analogue models and case studies: Geological Society of London, v. 170, no. 6, p. 893–904, doi:10.1144/jgs2013-012.

Santolaria, P., B. C. Vendeville, F. Graveleau, R. Soto, and A. Casas-Sainz, 2015, Double evaporitic décollements: Influence of pinch-out overlapping in experimental thrust wedges: Journal of Structural Geology, v. 76, p. 35–51.

Sokoutis, D., J.-P. Burg, M. Bonini, G. Corti, and S. Cloetingh, 2005, Lithospheric-scale structures from the perspective of analogue continental collision: Tectonophysics, v. 406, p. 1–15, doi:10.1016/j.tecto.2005.05.025.

Soleimany, B., T. Nalpas, and F. Sàbat, 2013, Multidetachment analogue models of fold reactivation in transpression: The NW Persian Gulf: Geologica Acta, v. 11, no. 3, p. 265–276, doi:10.1344/105.000001870.

Stewart, I. J., 1993, Structural controls on the Late Jurassic age shelf system, Ula trend, Norwegian North Sea *in* J. R. Parker, ed., Petroleum Geology of Northwest Europe: Proceedings of the 4th Conference, London, Geological Society, January 1, 1993, p. 469–483, doi:10.1144/0040469.

Tron, V., and J.-P. Brun, 1991, Experiments on oblique rifting in brittle-ductile systems: Tectonophysics, v. 188, no. 1–2, p. 71–84, doi:10.1016/0040-1951(91)90315-J.

Tvedt, A. B. M., A. Rotevatn, and C. A.-L. Jackson, 2016, Supra-salt normal fault growth during the rise and fall of a diapir: Perspectives from 3D seismic reflection data, Norwegian North Sea: Journal of Structural Geology, v. 91, p. 1–26, doi:10.1016/jsg2016.08.001.

Weijermars, R., M. P. A. Jackson, and B. Vendeville, 1993, Rheological and tectonic modeling of salt provinces, Tectonophysics, v. 217, p. 627–651, doi:10.1016/0040-1951(93)90208-2.

Wijns, C., R. Weinberg, K. Gessner, and L. Moresi, 2005, Mode of crustal extension determined by rheological layering: Earth and Planetary Science Letters, v. 236, no. 1, p. 120–134.

Willingshofer, E., D. Sokoutis, and J.-P. Burg, 2005, Lithosphere-scale analogue modelling of collision zones with a pre-existing weak zone, *in* D. Gapais, J. P. Brun, and P. R. Cobbold, eds., Deformation mechanisms, rheology and tectonics: From minerals to the lithosphere, Geological Society, London, Special Publication 2005, v. 243, no. 43, p. 277–294.

Wilson, P., G.M. Elliott, R. L. Gawthorpe, C. A.-L. Jackson, L. Michelsen, and I. R. Sharp, 2013, Geometry and segmentation of an evaporate-detached normal fault array: 3D seismic analysis of the southern Bremstein Fault Complex, offshore mid-Norway: Journal of Structural Geology, v. 51, p. 74–91, doi:10.1016/j.jsg.2013.03.005.

Withjack, M. O., and S. Callaway, 2000, Active normal faulting beneath a salt layer: An experimental study of deformation patterns in the cover sequence: AAPG Bulletin, v. 84, no. 5, p. 627–651.